JSR Publications

Available Online

J. Sci. Res. **13** (2), 679-694 (2021)

JOURNAL OF SCIENTIFIC RESEARCH

www.banglajol.info/index.php/JSR

DFT Study of Efinaconazole, an Antifungal Drug and Its Molecular Docking against a Holoenzyme (pdb id: 3IDB)

J. Hossen*, T. K. Pal

Department of Chemistry, Rajshahi University of Engineering & Technology, Rajshahi-6204, Bangladesh

Received 28 January 2021, accepted in final revised form 11 April 2021

Abstract

Efinaconazole (ECZ) is an antifungal drug. Various non-covalent interactions between ECZ and a holoenzyme (protein id: 3idb) has been investigated through computational study. The structure of ECZ was optimized using density functional theory (DFT) applying B3LYP/6-311G+(d,p) method. HOMO, LUMO, chemical hardness and softness, several thermochemical parameters, electrostatic potential surface, vibrational spectrum, total energy, and maximum internal force and maximum internal displacement with respect to optimization step number have been determined. The optimized ECZ ligand was subjected to molecular docking against the protein 3idb in Autodock Vina program. The different non-covalent interactions in the ligand-protein complex were visualized in BIOVIA Discovery Studio Visualizer. Various surface plots such as hydrogen bonds, ionizability, SAS, hydrophobicity, aromatic and charge surfaces were excerpted. ECZ molecule forms three strong hydrogen bonds with amino acid residues of the holoenzyme. In addition to this, it is significantly capable to form several other bonds which strengthen the ligand-protein interaction. The result showed that the ECZ molecule posed considerable binding affinity against the macromolecule.

Keywords: Efinaonazole; DFT; Molecular docking; 3idb; Ligand-protein complex.

doi: http://dx.doi.org/10.3329/jsr.v13i2.51731 J. Sci. Res. **13** (2), 679-694 (2021)

1. Introduction

Onychomycosis is a nail infectious disease caused by fungus in adults that is challenging to treat due to the deep location of the infection under the densely keratinized nail plate. Keratin sympathy influences the therapeutic activity of topical medicaments. For effectiveness, topical medicines must infiltrate into the nail bed and retain their antifungal efficacy within the nail matrix, both of which are unfavorably affected by keratin binding [1]. A recent study investigated efinaconazole (ECZ) as a new topical antifungal drug for onychomycosis. ECZ molecule has low keratin affinity which boost its high nail permeability and potent fungicidal activity in the presence of keratin which plays a vital role to its usefulness in onychomycosis [2]. The *in vitro* antifungal activity of ECZ was assessed in clinical isolates of *Trichophyton mentagrophytes*, *Trichophyton rubrum* and

* *Corresponding author*: jewelhossenruet@gmail.com

Candida albicans. ECZ has broad spectrum antifungal activity that may have applications in onychomycosis infection treatment [3]. Valeant Pharmaceuticals International developed a non-lacquer 10% topical solution of ECZ which received its first worldwide appreciation in Canada in October 2013 for onychomycosis treatment. The mechanism of action of ECZ as an antifungal medicine, seems to be analogous to that of other antifungal triazoles [4]. Application of 10% solution of ECZ daily once has been proved to be effective in the treatment of nail's fungal infection [5-7]. 3idb is a holoenzyme protein having two chain in structure. Chain A is known as cyclic adenosine monophosphate (cAMP)-dependent protein kinase (PKA) catalytic subunit alpha and chain B is known as cAMP-dependent protein kinase type II-beta regulatory subunit [8, 9]. The subunit A is put down by two classes of functionally non-redundant regulatory (R) subunits, RI and RII. Unlike RI subunits, RII subunits are both substrates and inhibitors. RIIbeta holoenzyme is a target for developing isoform-specific agonists and/or antagonists [8]. cAMP-dependent PKA is one of the best characterized members of the large PKA superfamily [10]. It was one of the first protein kinases discovered, sequenced, cloned, and the first PKA for which a crystal structure was solved [11]. It is present in every cell [12]. It thus serves in many ways as a prototype for the entire PKA superfamily which represents approximately 2 percent of the human genome. cAMP is an ancient stress response signal; for example, it is a universal indicator of glucose deprivation. Whereas, in bacteria the cAMP second messenger is related to the catabolite gene activator protein, in mammals it is associated primarily to the activation of PKA. PKA is ubiquitous in mammalian cells, and regulates multifaceted pathways [11]. No or very few studies have been found which investigate the DFT of ECZ molecule and its non-bonding interactions with 3idb protein through molecular docking which is the primary concern of this work.

2. Computational Methods

2.1. *Optimization of ECZ using DFT calculations*

The Efinaconazole (ECZ) molecule was firstly drawn in GaussView (version 6.0.16) [13] and then it was subjected to subsequent calculation. DFT calculations were performed using Gaussian 09 [14]. The structures of ECZ was fully optimized utilizing DFT employing B3LYP (Becke, 3-parameter, Lee–Yang–Parr) hybrid functional with the 6-311G+(d,p) basis set. The vibrational frequency of the ECZ molecule was also determined using the same level of theory. Internal electronic energy, enthalpy, Gibbs free energy and dipole moment were investigated for the molecules. Energetics data of a system exploiting Gaussian 09 are produced by solving traditional thermodynamic and quantum mechanical equations. Contributions from each of translational (E_t), rotational (E_r), vibrational (E_v) and electronic motions (E_e) are considered to estimate the thermodynamic parameters of a system. Sum of electronic and thermal energies in a molecule is represented by the following equation [14].

Sum of electronic and thermal energies = $\varepsilon_0 + E_{tot}$

Where ε_0 is the total electronic energy for a given system and E_{tot} is the correction to internal thermal energy when $E_{tot} = E_t + E_r + E_v + E_e$. Similarly,

Sum of electronic and thermal enthalpies = $\varepsilon_0 + H_{corr}$

Sum of electronic and thermal free energies = $\varepsilon_0 + G_{corr}$

Where H_{corr} and G_{corr} are the thermal corrections for enthalpy and Gibbs free energy for the given system respectively.

Calculation of frontier molecular orbitals was also conducted in conditions mentioned above. Correlating ionization potential (IP) to HOMO and electron affinity (EA) to LUMO, according to Koopmans theorem, chemical hardness (η) and softness (S) of the drug were calculated according to the equations below [15].

$$\text{Hardness } (\eta) = \frac{\text{LUMO-HOMO}}{2}$$

$$\text{Softness } (S) = \frac{1}{\eta}$$

2.2. *Preparation of protein*

Crystal structure of the protein (PDB ID: 3IDB) was downloaded from Protein Data Bank (https://www.rcsb.org/structure/3IDB). Prior to docking, heteroatoms, lipids and water molecules (as applicable) were eliminated from the crystal structure of the macromolecule using BIOVIA discovery studio software [16]. Geometry and energy minimization of the crystal structure were carried out with Swiss-PDB Viewer (v 4.1.0) employing GROMOS96 force field [17]. After that, the ligand and protein structures were individually saved as .pdb files in a directory.

2.3. *Binding site and molecular docking*

The active binding pocket and its size of the protein was predicted using CASTp (Computed Atlas of Surface Topography of proteins) [18] which found the largest pocket area and volume to be 1602.8 $Å^2$ and 2693.7 $Å^3$ respectively. Fig. 1 illustrates the most favorable pocket areas and volumes alongside the amino acid residue chains. The colored region in the protein structure represented pocket area and volume. These information were used to generate the grid boxes during molecular docking.

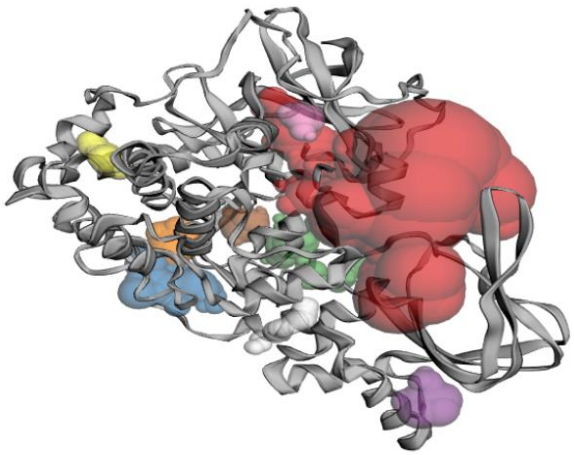

Fig. 1. Possible binding sites (pockets) with corresponding pocket size (in different colors) in the protein structure.

Molecular docking is a method that foretells preferred placement of a compound bound to another one (like protein) during the formation of a stable complex and finds its frequent application in *in silico* pharmaceutical drug design [19]. Current approaches of docking involve pose prediction, employing docking algorithms and energy-based scoring that identify the best binding mode of a drug to the active site of a desired protein, i.e. thermodynamically most favorable conformations. Lower free energy means better ligand–protein binding [20-22]. The two most common docking algorithms are flexible and rigid. In flexible docking, either one or both of the molecules are considered as flexible objects, whereas rigid docking does not allow conformational change of the ligand and protein, thereby accounting them as rigid solid objects [23,24]. In the current work, flexible docking of the ligand–protein entities were accomplished using Autodock Vina [25]. In performing flexible docking, ligand molecules were kept flexible and the protein was kept rigid. The grid box was constructed in such way that it covered the volume corresponding to the ligand protein molecules. The dimensions of grid box were chosen as follows: 199, 205 and 143 Å towards X, Y and Z coordinates respectively. Detailed analysis of various non-covalent interactions between the ligand and protein was explored using Discovery Studio 4.5 (2019) and LigPlot+ (version 1.4.5) [26].

3. Results and Discussion

3.1. *Structure optimization and geometry of ECZ*

Table 1 presents selected bond lengths, bond angles, and dihedral angles for optimized ECZ molecule calculated in the gas-phase using DFT with the B3LYP functional and 6-311G+(d,p) basis set. For the compound, the bond lengths, bond angles and dihedral angles agree very well. The structure of the ECZ molecule optimized in the above conditions is shown in Fig. 2. The distances of O-H bond and O-C are 0.973 and 1.422 Å

respectively which shows good agreement with another literature values (0.963 and 1.375) calculated in the same criteria [27]. Two C-F bond distances are around similar values 1.352 and 1.350 Å. The distance of N37-C14 bond is 1.480 Å which has similarity with literature obtained by x-ray [28]. C12-C13 and C12-C14 single bonds' distances are 1.552 and 1.599 Å respectively, and C34=C41 double bond's length is 1.334 Å, these values show very good consistency with literature value [29]. The other bonds have also congruous values as well.

Total energy change (Kcal/mole) and associated root mean square gradient (Kcal/Angstrom), maximum internal force change (Hartree/Bohr-radians) and maximum internal displacement in each step of optimization of the ECZ are shown in the Fig. 3. The total energy vs step number reveals that the structure has been optimized in 21 steps and reached gradually to the minimal energy value at the last step (Fig. 3a). Initially the decrement of energy was rapid but after fourth step, it was gradually slower to the lowest value. The rms gradient norm curve support the former very well. In addition to total energy plot, the maximum internal force (Fig. 3c), maximum internal displacement (Fig. 3d) pattern revealed that the ECZ molecule has reached the lowest possible energy state. The values of some thermochemistry parameters of the ECZ molecule calculated in the above mentioned DFT method are provided in Table 2.

Table 1. Selected bond lengths (Å), bond angles (degree) and dihedral angles (degree) of ECZ (in the gas-phase) obtained from the optimization using DFT/B3LYP/6-311G+ (d,p) at 298.15 K.

Bond length (Å)		Bond angle (degree)		Dihedral angle (degree)	
C34=C41	1.334	H42-C41-H43	116.890	H43-C41-C34-C30	2.390
N37-C14	1.480	C32-C34-C41	123.419	C28-N37-C14-C12	108.189
O15-C12	1.422	C28-N37-C29	111.171	N37-C14-C12-C4	163.125
F10-C5	1.350	C13-C14-N37	95.066	N37-C14-C12-O15	42.307
F9-C1	1.351	H38-C13-H40	107.775	O15-C12-C13-N17	65.877
H15-O16	0.973	H16-O15-C12	103.621	C12-C13-N17-N18	128.278
C12-C14	1.599	C4-C5-F10	121.210	C12-C4-C5-F10	0.999
N17-N18	1.361	C13-N17-N18	119.675	H23-C20-N17-C13	3.275
N21=C20	1.322	C19-N21-C20	102.860	H22-C19-N18-N17	179.887
C12-C13	1.552	N17-C13-H38	105.501	C3-C2-C1-C6	0.654

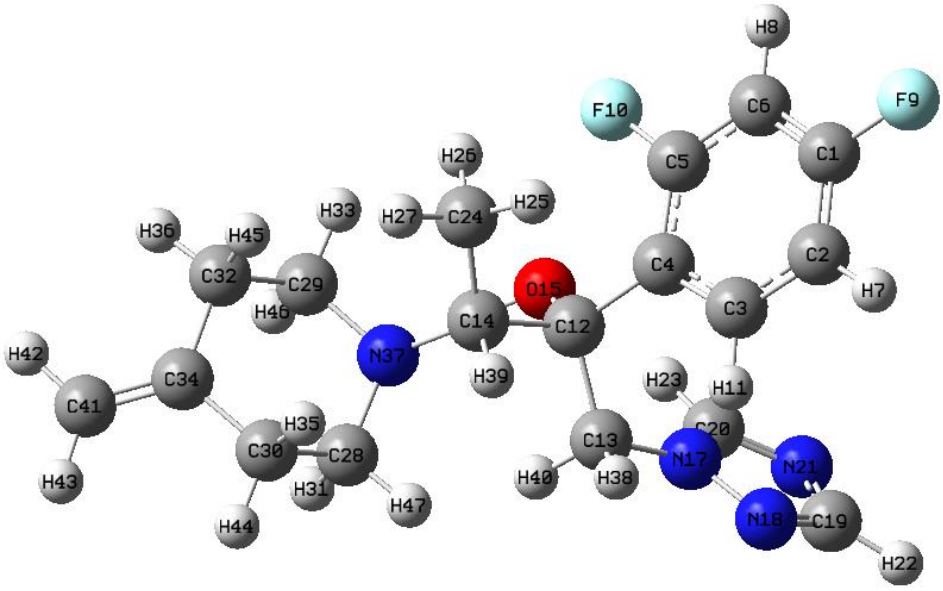

Fig. 2. Optimized structure of the ECZ molecule.

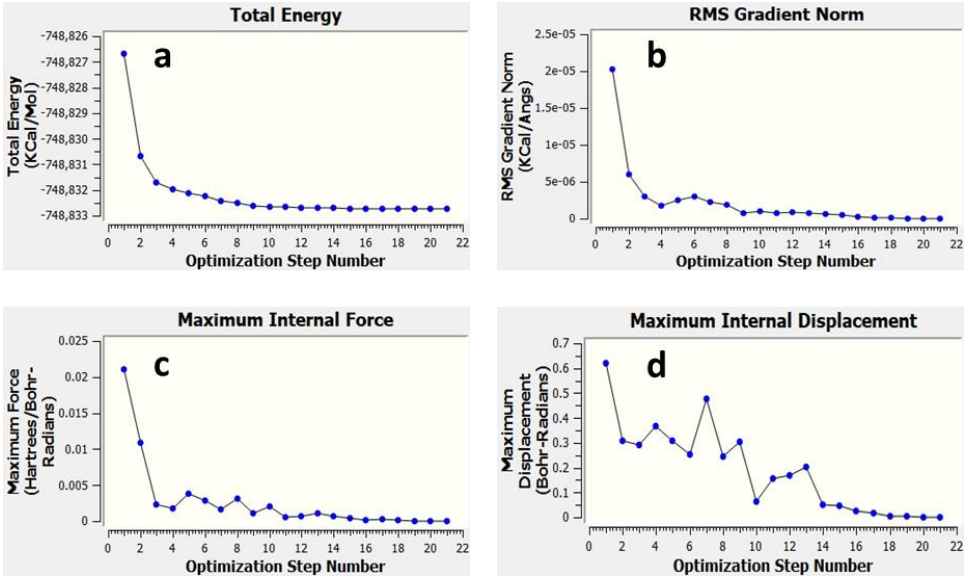

Fig. 3. (a) Total energy change (Kcal/mol), (b) Root mean square gradient norm (Kcal/Angs), (c) Maximum internal force change (Hartree/Bohr-radians) and (d) Maximum internal displacement in each step of optimization of the ECZ molecule.

Table 2. Values of some physical parameters (at 298.15 K and 1 atmosphere).

Dipole moment	6.0226 Debye
Zero-point correction	0.384 Hartree
Thermal correction to Energy	0.407 Hartree
Thermal correction to Enthalpy	0.408 Hartree
Thermal correction to Gibbs Free Energy	0.331 Hartree
Sum of electronic and zero-point Energies	-1192.956 Hartree
Sum of electronic and thermal Energies	-1192.933 Hartree
Sum of electronic and thermal Enthalpies	-1192.932 Hartree
Sum of electronic and thermal Free Energies	-1193.009 Hartree
Heat Capacity (Cv)	88.138 Cal/Mol-Kelvin
Entropy (S)	161.537 Cal/Mol-Kelvin

3.2. *Vibrational spectrum*

Vibrational spectrum of optimized ECZ molecule is shown in the Fig. 4. The spectrum showed the characteristic bands of the corresponding functional groups. The sharp peak at 3645 cm^{-1} is the characteristic peak of stretching vibration for hydroxyl (OH) group. The bands at 3205 and 3124 cm^{-1} correspond to asymmetric stretching of $=CH_2$ and CH_3 group respectively. Peaks at 3070 and 3009 cm^{-1} are attributed for the asymmetric and symmetric stretching of CH_2 groups respectively. The C=C showed characteristic band at 1707 cm^{-1}, and benzene ring and nitrogen containing five-membered ring showed corresponding bands at 1653 and 1535 cm^{-1} respectively. The small band at 1312 cm^{-1} is the characteristic to NCH scissoring. The C-O bond shows the small band at 1113 cm^{-1}. The band at 989 cm^{-1} is characteristic to C-F bond stretching and that at 640 cm^{-1} is to OH bending.

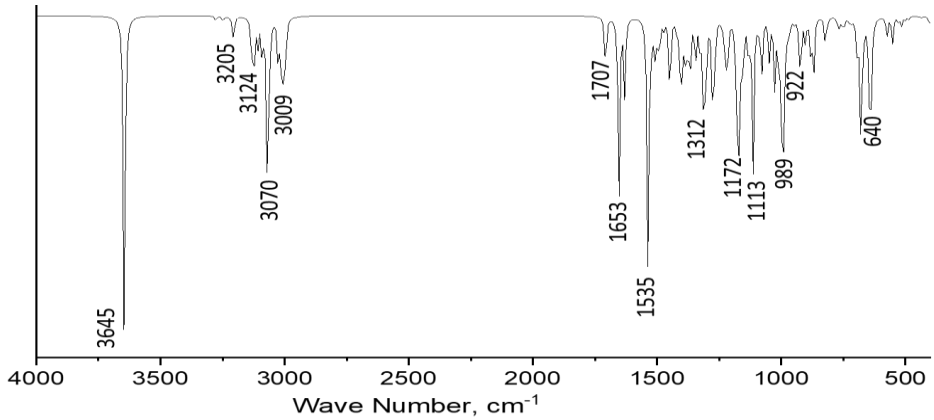

Fig. 4. Vibrational spectrum of ECZ molecule calculated by DFT method with B3LYP/6-311G+(d,p).

3.3. *Frontier molecular orbitals*

Highest occupied molecular orbital (HOMO) and lowest unoccupied molecular orbital (LUMO) are generally known as Frontier molecular orbitals (FMO). The HOMO and LUMO are the two most important molecular orbitals. Energies of the FMO are significant to determine biochemical reactivity and the extent to which a drug interacts with a certain receptor [30]. Even, only the HOMO energy along can be a vital determinant to find a liaison between a class of drug's activity and their electronic configuration [31]. In chemistry, FMO is an important concept, and molecular orbital theory is utilized extensively to describe chemical behavior of substances. Apart from these, it also offers an indispensable conceptual construct to describe other phenomenon involving molecular electronic structure including charge transfer processes, magnetism, photoexcitation, kinetics and molecular electronics [32]. According to Koopmans' theorem, experimental ionization potential (IP) is the negative of HOMO energy and similarly for N-electron system electron affinity (EA) is equal to the negative of LUMO energy, assuming that the orbitals do not relax [32]. Pictorial views of HOMO, HOMO-1, LUMO and LUMO+1 of ECZ molecule is shown in Fig. 5.

A molecule's electron donating and receiving ability can be defined in terms of HOMO and LUMO energy. These molecular orbitals play vital role in electronic and optical properties, photochemical reaction, luminescence, quantum chemistry, uv-visible spectrum and pharmaceutical studies [33, 34]. The energy gap between HOMO and LUMO predicts of a molecule's kinetic and chemical stability [35]. Larger FMO gap agreements with high kinetic stability, but low chemical reactivity, as it is energetically unpropitious for an electron to elevate from a low-energy HOMO to a relatively high-lying LUMO [36, 37].

HOMO orbitals are mostly localized on the carbon and nitrogen atoms of the six membered heterocyclic ring with an extented lobe to C=C double bonded side chain, and oxygen atom, and partially localized on the benzene cycle (Fig. 5a). On the other hand, the LUMO orbitals are mainly locaized on the benzene ring and slightly on the flurine atoms (Fig. 5b). The HOMO-1 orbitals are distributed over the benzene ring, flurine atoms, nitrogen containing five membered ring and also on the C=C double bonded side chain (Fig. 5c). But LUMO+1 lobes are bestrewn primarily over the bezbene ring with both flurine atoms (Fig. 5d). The calculated energy values of HOMO and LUMO orbitals are -0.23301 eV and -0.03779 eV respectively (Fig. 6). The HOMO–LUMO gap is related to the chemical hardness and softness of a molecule [38, 39]. The FMO's energy gap (LUMO–HOMO) of the mentioned organic molecule was found to be 0.19522 eV. The lower value of the energy gap showed that the studied molecule has high chemical reactivity, biological activity and polarizability. The calculated chemical hardness (η) and softness (S) of the ECZ molecule is 0.09761 and 10.24485 respectively.

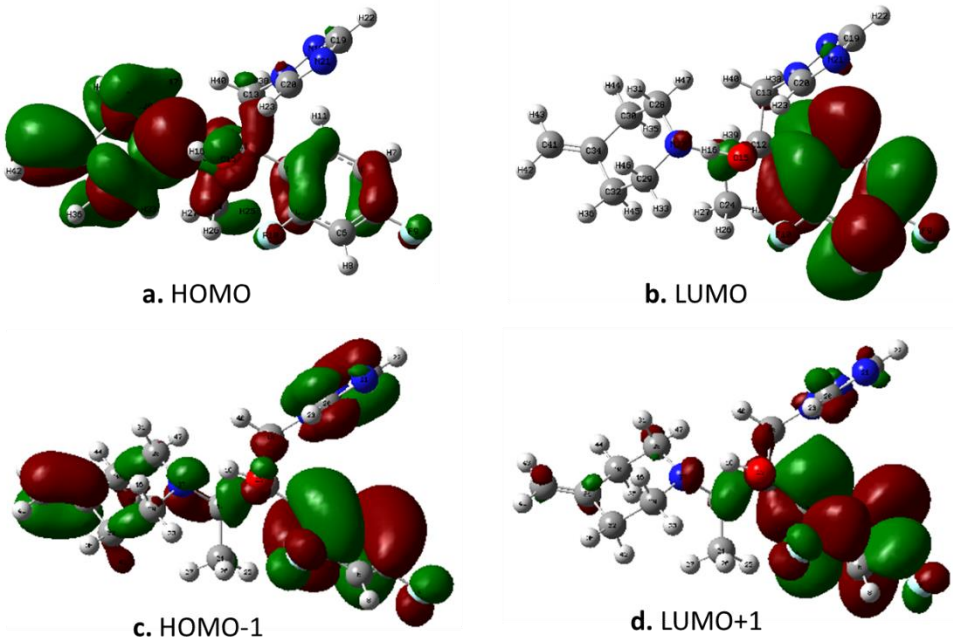

Fig. 5. (a) Highest Occupied Molecular Orbital (HOMO), (b) Lowest Unoccupied Molecular Orbital (LUMO), (c) HOMO-1 and (d) LUMO+1 Frontier Orbitals.

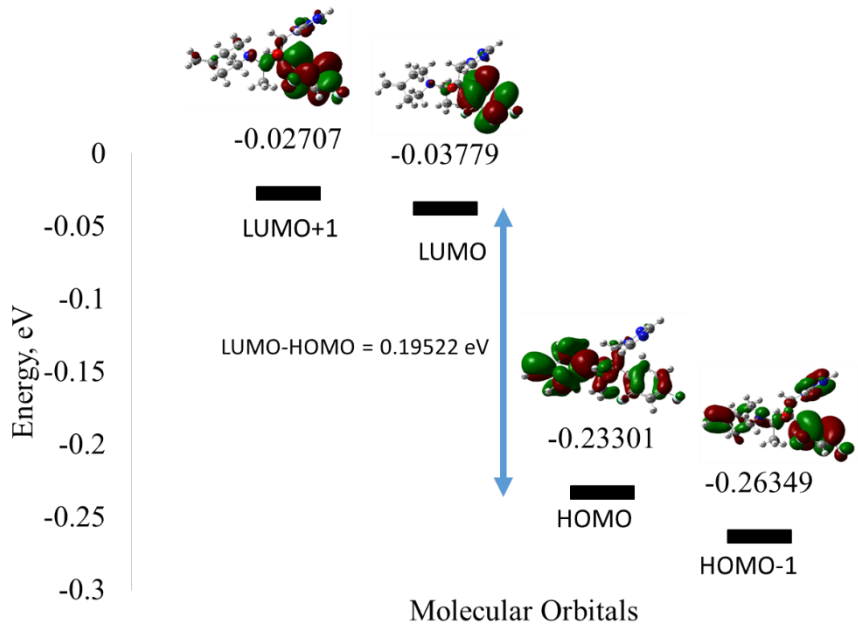

Fig. 6. Energy distribution of four frontier orbitals and LUMO-HOMO energy gap.

3.4. *Electrostatic potential surface*

The molecular electrostatic potential (MEP) is used to predict the relative reactivity positions of a molecule for electrophilic and nucleophilic attack. The electrostatic potential is considered predictive of chemical reactivity because regions of negative potential are expected to be sites of protonation and nucleophilic attack, while regions of positive potential may indicate electrophilic attack. The electrostatic potential (electron density) surface of the ECZ molecule is shown in Fig. 7. The color code of the compound lies in the range of $-5.681e^{-2}$ to $+5.681e^{-2}$. Red and blue color in the MEP surface point to more electron rich (negative) and electron poor region (positive) respectively. Nitrogen, oxygen and fluorine positioned surfaces are colored red indicating electron rich area and the other region are slightly blue indicating positivity area.

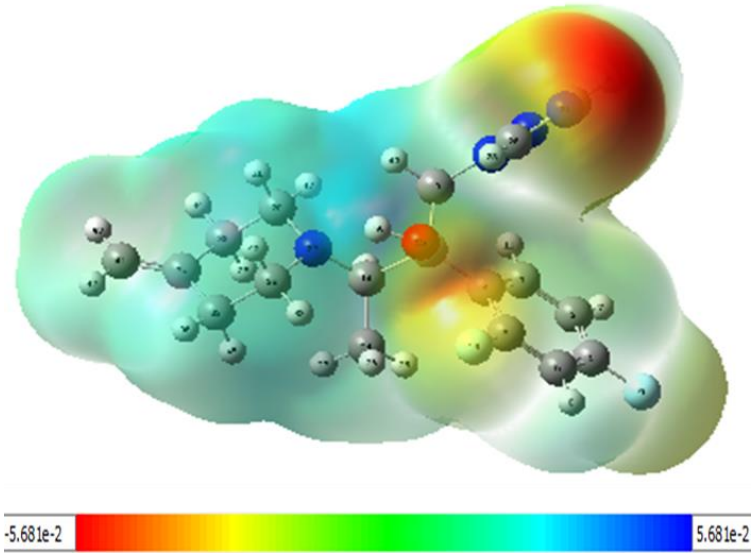

Fig. 7. 3D-representation of the electrostatic potential (electron density) surface around the molecule calculated using the Density Functional Theory at B3LYP level of theory and 6-311G+(d,p) basis set.

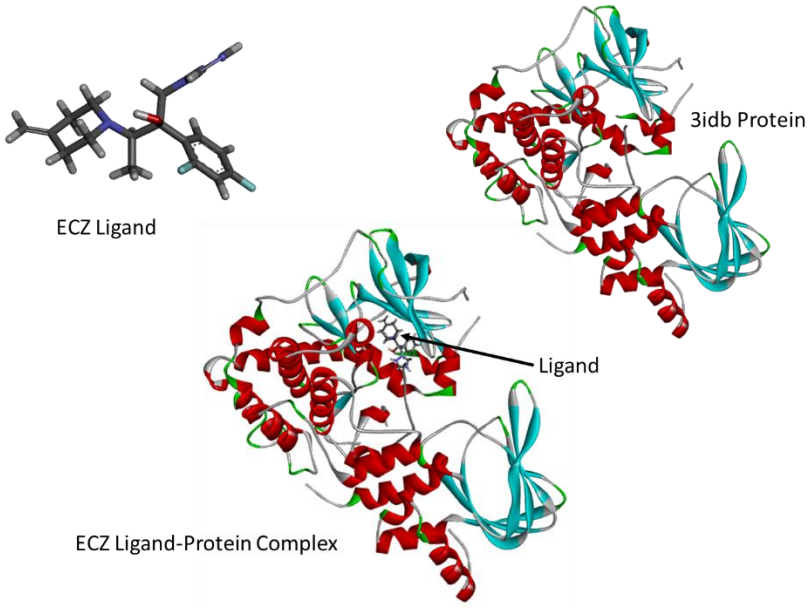

Fig. 8. Ligand (ECZ), protein (3idb) and ligand-protein complex.

3.5. *Molecular docking*

AutoDock Vina platform was applied for docking purpose throughout the study. Even though this program has been regarded as quite accurate for calculating binding score and binding poses compared to other available docking platforms [40], it still suffers from major restrictions among which does not account for backbone flexibility in receptors [41]. Therefore, we conducted multiple receptor conformation (MRC) based molecular docking which is a different pathway to receptor flexibility to study the aftermath of receptor's conformational change on binding score and poses. The bare ligand and protein, and the docked ligand-protein complex are presented in the Fig. 8. Binding free energy of ECZ-protein complex was calculated 8.7 Kcal/mol. Analysis of ECZ-3idb complex reveals that several hydrogen bonds have formed in drug-receptor interaction (Fig. 9). Residues such as Phe54 (2.77 Å), Gly55 (2.46 Å) and Asp184 (2.61 Å) make strong hydrogen bonds with the ligand. Presence of fluorine atoms in the ligand contributes in the formation of hydrogen bonds. In addition to the hydrogen bonds, several other interactions are also present here, such as carbon hydrogen bond, halogen (fluorine), pi-cation, alkyl, pi-alkyl and van der Waals interactions which strengthen drug-receptor interactions [42]. The non-bonding interactions between the ligand and macromolecule is reported in Table 3.

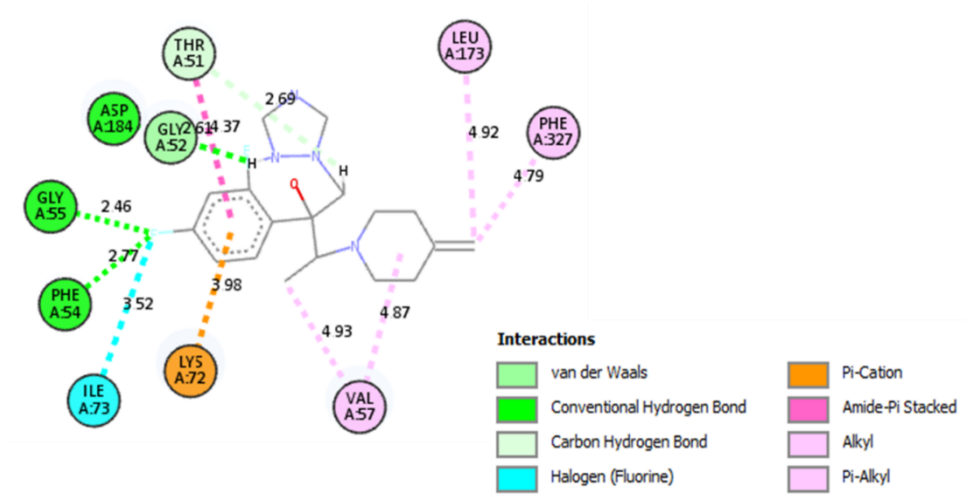

Fig. 9. 2D Representation of ligand-protein interaction.

Table 3. Name, distance, category and type of ligand-protein interactions.

Name	Distance	Category	Type
HN – ASP184	2.60608	Hydrogen Bond	Conventional Hydrogen Bond
F – NH:PHE54	2.76832	Hydrogen Bond	Conventional Hydrogen Bond
F – NH:GLY55	2.45708	Hydrogen Bond	Conventional Hydrogen Bond
H7 – O:THR51	2.69136	Hydrogen Bond	Carbon Hydrogen Bond
H8 - N (Intra-ligand)	1.96638	Hydrogen Bond	Carbon Hydrogen Bond
N – F (Intra-ligand)	3.18115	Halogen	Halogen (Fluorine)
F – C:PHE54	3.23853	Halogen	Halogen (Fluorine)
F – C:GLY55	3.39995	Halogen	Halogen (Fluorine)
F – O:ILE73	3.52192	Halogen	Halogen (Fluorine)
Pi – NZ:LYS72	3.98453	Electrostatic	Pi-Cation
C – VAL57	4.9279	Hydrophobic	Alkyl
C – LEU173	4.91561	Hydrophobic	Alkyl
0 – VAL57	4.87405	Hydrophobic	Alkyl
Pi – LYS72	4.87382	Hydrophobic	Pi-Alkyl
Pi-C – PHE327	4.79172	Hydrophobic	Pi-Alkyl

3.6. *Hydrogen bonds, ionizability, solvent accessible surface (SAS) and hydrophobicity surfaces*

The post-docked ligand-protein complex was opened in Discovery Studio Client program, then displayed the mutual interactions and created different surfaces around the ligand [43]. Fig. 10 (a-f) presented different receptor surfaces, such as H-bonds donor/acceptor, ionizability basic/acidic, solvent accessibility surface (SAS), hydrophobicity, aromatic edge/face and interpolated charge surfaces.

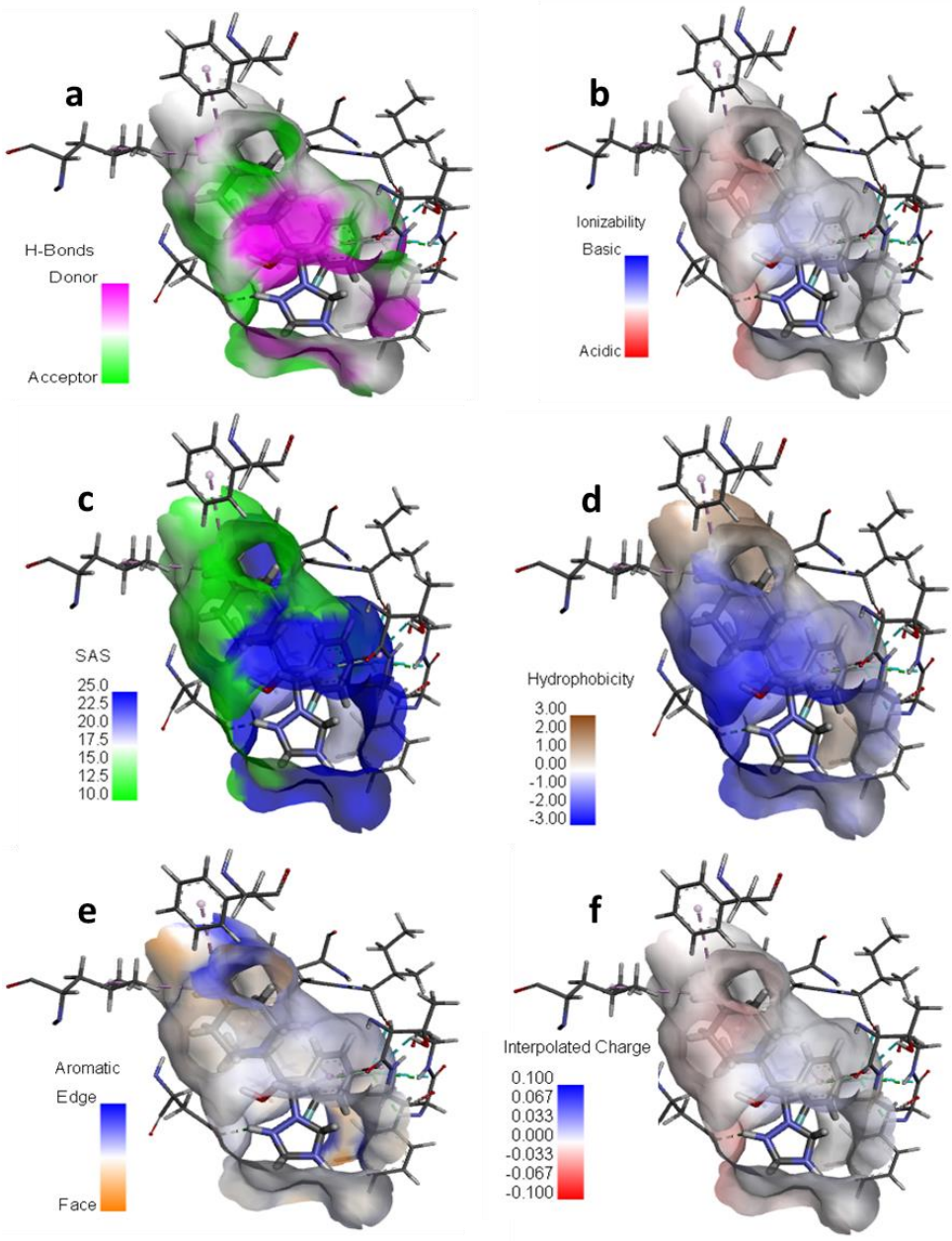

Fig. 10. The schematic representation of (a) H-bond, (b) Ionizability, (c) Solvent accessible surface (SAS), (d) Hydrophobicity, (e) Aromatic and (f) Interpolated charge surfaces of 3idb around ECZ molecule.

The H-bond surface denotes the hydrogen atom donor area in pink color and acceptor area in green color of the amino acid residues around ligand (Fig. 10a). Here fluorine atoms play a pivotal role in formation of hydrogen bonds. The basic and acidic propensity of the macromolecule was indicated with the ionization surface (Fig. 10b, basic/blue color and acidic/red color). The solvent accessibility surface (SAS) or solvent-accessible surface area (SASA) is the surface area of a biomolecule (like protein) that is achievable to a solvent [44]. The high accessible area especially the polar region is colored blue and poor accessible area is colored green (Fig. 10b). In the current case, the SAS surface showed that Gly52, Gly55, Val57 and Asp184 residues pose high SAS proclivity. The hydrophobicity surface indicated that the current receptor around the ligand has hydrophilicity features. Also, the aromatic edge/face surface (Fig. 10e, blue/orange = edge/ face) and interpolated charge surface (Fig. 10f, blue/red = positive/ negative value), have been illustrated on the basis of docking result of 3idb macromolecule and ECZ ligand.

4. Conclusion

In this article, the ligand ECZ molecule was fully optimized through DFT calculation using B3LYP/311G+(d,p) method. The HOMO-LUMO molecular orbital energies, and the physical descriptors such as hardness, softness derived from HOMO and LUMO energies and MEP surface of the entitled ECZ ligand suggested that it was chemically active with its low hardness and high softness. So, its electron cloud is polarized or distorted in an electric field. Molecular docking between the ligand molecule and the protein (3idb) shows considerably favorable free energy of binding. Several non-bonding interactions between the ECZ molecule and the amino acid residues of the macromolecule have been observed which support strong affinity of the ligand toward the protein. The ECZ molecule having the electronegative fluorine atoms possesses competence to non-covalently bind with the macromolecule 3idb and inhibit its action. So, it can be concluded that the ligand is able to pose as a drug against the protein discussed.

Acknowledgment

The authors acknowledge to Red-Green Research Centre, Dhaka, Bangladesh, which provided an opportunity of hand on training on theories and software of computational chemistry.

References

1. M. A. Kamal, T. Nabekura, and S. Kitagawa, Chem. Pharm. Pull. **53**, 441 (2005). https://doi.org/10.1248/cpb.53.441
2. K. Sugiura, N. Sugimoto, S. Hosaka, M. Katafuchi-Nagashima, Y. Arakawa, Y. Tatsumi, W. J. Siu, and R. Pillai, Antimicrob. Agents Chemother. **58**, 3837 (2014). https://doi.org/10.1128/aac.00111-14
3. W. J. J. Siu, Y. Tatsumi, H. Senda, R. Pillai, T. Nakamura, D. Sone, and A. Fothergill, Antimicrob. Agents Chemother. **57**, 1610 (2013). https://doi.org/10.1128/AAC.02056-12

4. T. Patel and S. Dhillon, Drugs **73**, 1977 (2013). https://doi.org/10.1007/s40265-013-0152-x
5. M. Jarratt, W. J. Siu, E. Yamakawa, N. Kodera, R. Pillai, and K. Smith, J. Drugs Dermatol. **12**, 1010 (2013).
6. P. Rich, J. Drugs Dermatol. **14**, 58 (2015). https://doi.org/10.17116/klinderma2015158-62
7. D. A. Rodriguez, J. Clin. Aesthet. Dermatol. **8**, 24 (2015).
8. S. H. Brown, J. Wu, C. Kim, K. Alberto, and S. S. Taylor, J. Mol. Biol. **393**, 1070 (2009). https://doi.org/10.1016/j.jmb.2009.09.014
9. S. H. Brown, C. Y. Cheng, S. A. Saldanha, J. Wu, H. B. Cottam, B. Sankaran, and S. S. Taylor, ACS Chem. Biol. **8**, 2164 (2013). https://doi.org/10.1021/cb400247t
10. S. S. Taylor and E. Radzio-Andzelm, in Handbook of Cell Signaling (Academic Press, 1461, 2010). https://doi.org/10.1016/B978-0-12-374145-5.00179-0
11. R. A. Bradshaw and E. A. Dennis, Handbook of Cell Signaling (Academic press, 2009). https://doi.org/10.1016/B978-0-12-374145-5.00001-2
12. Y. Asaoka, In Vitamins & Hormones, Vol. 88 (Academic Press, 2012) pp. 293. https://doi.org/10.1016/B978-0-12-394622-5.00013-4
13. R. Dennington, T. A. Keith, and J. M. Millam, Gauss View, version 6.0. 16. (Semichem Inc. Shawnee Mission KS. 2016).
14. Gaussian 09 Revision D.01 (Gaussian Inc., Wallingford CT, 2009). http://www.gaussian.com
15. R. G. Pearson, Proc. Natl. Acad. Sci. **83**, 8440 (1986). https://doi.org/10.1073/pnas.83.22.8440
16. Discovery Studio Modeling Environment, version 4.5. (Accelrys Software Inc., San Diego, 2019).
17. N. Guex, M. C. Peitsch, and T. Schwede, Electrophoresis **30**, 162 (2009). https://doi.org/10.1002/elps.200900140
18. J. Dundas, Z. Ouyang, J. Tseng, A. Binkowski, Y. Turpaz, and J. Liang, Nucleic Acids Res. **34**, W116 (2006). https://doi.org/10.1093/nar/gkl282
19. T. Kaur, A. Madgulkar, M. Bhalekar, and K. Asgaonkar, Curr. Drug Discov. Technol. **16**, 30 (2019). https://doi.org/10.2174/1570163815666180219112421
20. R. Thomsen and M. H. Christensen, J. Med. Chem. **49**, 3315 (2006). https://doi.org/10.1021/jm051197e
21. D. A. Gschwend, A. C. Good, and I. D. Kuntz, J. Mol. Recognit. **9**, 175 (1996). https://doi.org/10.1002/(SICI)1099-1352(199603)9:2%3C175::AID-JMR260%3E3.0.CO;2-D
22. C. Fu, L. Zhao, X. Tan, J. Li, and X. Wang, J. Biomol. Struct. Dyn. **38**, 4607 (2019). https://doi.org/10.1080/07391102.2019.1680433
23. X. Zhou, Y. Wang, T. Hu, P. M. Or, J. Wong, Y. W. Kwan, D. C. Wan, P. M. Hoi, P. B. Lai, and J. H. Yeung, Phytomedicine **20**, 367 (2013). https://doi.org/10.1016/j.phymed.2012.09.021
24. I. Halperin, B. Ma, H. Wolfson, and R. Nussinov, Proteins **47**, 409 (2002). https://doi.org/10.1002/prot.10115
25. O. Trott and A. J. Olson, J. Comput. Chem. **31**, 455 (2010). https://doi.org/10.1002/jcc.21334
26. R. A. Laskowski and M. B. Swindells, J. Chem. Inf. Model. **51**, 2778 (2011). https://doi.org/10.1021/ci200227u
27. R. A. Mendes, B. L. Silva, R. Takeara, R. G. Freitas, A. Brown, and G. L. De Souza, J. Mol. Model. **24**, 101 (2018). https://doi.org/10.1007/s00894-018-3632-9
28. L. Morello, J. B. Love, B. O. Patrick, and M. D. Fryzuk, J. Am. Chem. Soc. **126**, 9480 (2004). https://doi.org/10.1021/ja049490b
29. A. Streitwieser, C. H. Heathcock, E. M. Kosower, and P. J. Corfield, Introduction to Organic Chemistry (Macmillan, New York 1992) **547 STR**.
30. A. Ali, M. Khalid, S. Abid, J. Iqbal, M. N. Tahir, A. R. Raza, and M. W. Paixão, Appl. Organomet. Chem. **34**, ID e5399 (2020). https://doi.org/10.1002/aoc.5399
31. S. H. Snyder and C. R. Merril, Proc. Natl. Acad. Sci. U. S. A. **54**, 258 (1965). https://doi.org/10.1073%2Fpnas.54.1.258
32. C. J. Cramer, Essentials of Computational Chemistry: Theories and Models (John Wiley & Sons, 2013).

33. S. A. Beyramabadi, M. Javan-Khoshkholgh, N. J. Ostad, A. Gharib, M. Ramezanzadeh, M. Sadeghi, and A. Morsali, J. Struct. Chem. **59**, 1342 (2018). https://doi.org/10.1134/S0022476618060136
34. S. Kumar, V. Saini, I. K. Maurya, J. Sindhu, M. Kumari, R. Kataria, and V. Kumar, PloS one, **13**, e0196016 (2018). https://doi.org/10.1371/journal.pone.0196016
35. E. Thomas, K. P. Vijayalakshmi, and B. K. George, J. Mol. Liq. **276**, 721 (2019). https://doi.org/10.1016/j.molliq.2018.12.034
36. M. M. Hoque, M. A. Halim, M. M. Rahman, M. I. Hossain, and M. W. Khan, J. Mol. Struct. **1054**, 367 (2013). https://doi.org/10.1016/j.molstruc.2013.10.011
37. A. Rahman, M. M. Hoque, M. A. Khan, M. G. Sarwar, and M. A. Halim, Springerplus, **5**, 146 (2016). https://doi.org/10.1186/s40064-016-1844-y
38. P. W. Ayers, Faraday Discussions, **135**, 161 (2007). https://doi.org/10.1039/B606877D
39. R. G. Parr and Z. Zhou, Acc. Chem. Res. **26**, 256 (1993). https://doi.org/10.1021/ar00029a005
40. Z. Wang, H. Sun, X. Yao, D. Li, L. Xu, Y. Li, S. Tian, and T. Hou, Phys. Chem. Chem. Phys. **18**, 12964 (2016). https://doi.org/10.1039/C6CP01555G
41. N. S. Pagadala, K. Syed, and J. Tuszynski, Biophys. Rev. **9**, 91 (2017). https://doi.org/10.1007/s12551-016-0247-1
42. G. Gayatri, J. Sci. Res. **13**(1), 253 (2021). https://dx.doi.org/10.3329/jsr.v13i1.48371
43. R. Krivák, L. Jendele, and D. Hoksza, *Proceedings of the 2018 ACM International Conference on Bioinformatics, Computational Biology, and Health Informatics*, 645 (2018). https://doi.org/10.1145/3233547.3233708
44. A. Ranjbar, M. Jamshidi, and S. Torabi, Eur. Rev. Med. Pharmacol. Sci. **24**, 7834 (2020). https://doi.org/10.26355/eurrev_202007_22288